https://doi.org/10.5194/egusphere-2025-714
Preprint. Discussion started: 4 March 2025

Corresponding author: Marcin.J.Kurowski@jpl.nasa.gov

The Diurnal Susceptibility of Subtropical Clouds to Aerosols

Marcin J. Kurowski[1], Matthew D. Lebsock[1], and Kevin M. Smalley[2]

[1]Jet Propulsion Laboratory, California Institute of Technology, Pasadena, California, USA.
[2]Lawrence Livermore National Laboratory, Livermore, California, USA.

Abstract. The diurnal susceptibility of clouds to aerosols is examined during the transition from subtropical stratocumulus to shallow cumulus regimes. Using large-eddy simulations, a six-day air mass evolution along a 3800-km observed trajectory from the coast of Peru toward the equator is analyzed. Pristine and polluted scenarios are simulated with forcing imposed from weather reanalysis. The polluted scenario exhibits stronger diurnal variations in cloud water, cloud fraction, and albedo, with enhanced entrainment and suppressed precipitation. The overall response of cloud properties and outgoing shortwave radiation to droplet number concentration follows a distinct diurnal pattern: strong positive adjustments dominate at night and in the morning, while weak negative adjustments prevail in the afternoon. This cycle is driven by the competition between precipitation suppression, which enhances cloud water and coverage, and entrainment drying, which depletes them. In polluted conditions, enhanced entrainment leads to a deeper and more decoupled boundary layer that cannot be sustained by surface fluxes in the afternoon, resulting in negative cloud adjustments. This entrainment enhancement is mediated by the sedimentation of cloud and precipitation water from the entrainment zone. While the Twomey effect dominates the diurnal average albedo response, the diurnal variation in the competing cloud adjustments lead to a near-neutral net adjustment effect, highlighting the critical role of diurnal processes in aerosol-cloud interactions.

1 Introduction

The interactions between aerosol and clouds represent one of the largest sources of uncertainties in the anthropogenic radiative forcing of Earth's climate (IPCC, 2021, 2022). The radiative effect of the collective set of changes to cloud morphology by aerosol is known as the Effective Radiative Forcing due to Aerosol Cloud Interactions ($\mathrm{ERF_{ACI}}$) (Wall et al., 2022), which is composed of a number of different cloud changes. The first order effect, often referred to as the Twomey effect (Twomey, 1977) posits that an increase in cloud droplet number (N_c) for fixed liquid water path results in a greater integrated water droplet cross sectional area and thus an increase in cloud optical depth (τ_c) and cloud albedo (A_c). The magnitude of the Twomey effect is thought to be relatively well understood (Quaas et al., 2020). However, second-order indirect effects, or cloud adjustments, result from changes to the cloud liquid water path ($\mathrm{LWP_c}$) and cloud cover fraction (f_c), where the domain

https://doi.org/10.5194/egusphere-2025-714
Preprint. Discussion started: 4 March 2025

mean liquid water path is LWP $= f_c$LWP$_c$. These cloud adjustments are less well understood. It was first thought that increases in N_c would inhibit the formation of precipitation and thus increase cloud lifetime (Albrecht, 1989; Pincus and Baker, 1994). More recently, it was suggested that increasing N_c can reduce LWP$_c$ through a decreased sedimentation efficiency causing an increase in liquid near the cloud top which enhances the efficiency of the entrainment of dry free-tropospheric air into the cloud layer (Bretherton et al., 2007; Ackerman et al., 2004). To quantify the various aerosol cloud interactions the sensitivity of the reflected shortwave flux ($F^{\uparrow}$) is often decomposed into three terms (Bellouin et al., 2020) representing changes in τ_c at fixed LWP$_c$ (S_N), additional changes in τ_c resulting from changes in LWP$_c$ at fixed N_c (S_{LWP})and changes in f_c at fixed τ_c (S_f)

$$\frac{\mathrm{dln}F^{\uparrow}}{\mathrm{dln}N_c} = \underbrace{\frac{\partial \mathrm{ln}F^{\uparrow}}{\partial \mathrm{ln}N_c}}_{\text{Twomey Effect}(S_N)} + \underbrace{\frac{\partial \mathrm{ln}F^{\uparrow}}{\partial \mathrm{lnLWP}_c}\frac{\mathrm{dlnLWP}_c}{\mathrm{dln}N_c}}_{\text{LWP adjustment}(S_{\mathrm{LWP}})} + \underbrace{\frac{\partial \mathrm{ln}F^{\uparrow}}{\partial f_c}\frac{\mathrm{d}f_c}{\mathrm{dln}N_c}}_{\text{fraction adjustment}(S_f)} \tag{1}$$

There is observational evidence for both increases and decreases in the LWP$_c$. For example, Han et al. (2002) use satellite data to show that clouds have positive, negative, and neutral sensitivity to aerosol in roughly equal proportions. It is also clear that the sign of the response is dependent on the cloud state. Lebsock et al. (2008) find that the LWP$_c$ tends to increase with increased N_c for precipitating clouds and decrease with increasing N_c for non-precipitating clouds. Evidence from ship-tracks show both positive and negative sensitivity (Ackerman et al., 2000; Coakley and Walsh, 2002), with the observation that the sign of the response is associated with the mesoscale cellular structure with open-celled regimes tending to have a positive response and closed-cells tending to have a negative response, presumably due to their differential propensity to precipitate (Christensen and Stephens, 2012). A recent review of polluted clouds down-wind of anthropogenic pollution sources finds a weak albeit slightly negative average response of LWP$_c$ to aerosol perturbations Toll et al. (2019). To the contrary, Manshausen et al. (2022) recently find a large positive increases in LWP$_c$ by using ship location data to find a large number of 'invisible' ship tracks, which are not readily identifiable in satellite imagery.

Observed positive correlations between aerosol optical depth and f_c have long been considered suspect due to the tendency to observe enhanced clear sky reflectance in the vicinity of clouds due to three dimensional radiative effects (Várnai and Marshak, 2009). For example, carefully controlling for the distance of an aerosol retrieval to the nearest cloud nearly halves the magnitude of the relationship between f_c and aerosol optical depth (Christensen et al., 2017). To entirely avoid the influence of artificial correlations, more recent observational studies have used either the observed N_c or a model derived aerosol field in place of the aerosol optical depth to derive the slope $\mathrm{d}f_c/\mathrm{dln}N_c$. Although the magnitude is highly uncertain, studies tend to find a positive correlation (Gryspeerdt et al., 2016; Wall et al., 2023).

Most observational satellite studies are based on visible and near infrared imager data with fixed diurnal sampling time therefore there are few hints as to the observed diurnal cycle of the cloud adjustments. A study of a South Atlantic shipping lane shows that Terra MODIS shows a larger positive LWP adjustment than Aqua MODIS, and the Terra/Aqua show positive/negative f_c adjustments (Diamond et al., 2020). The recent observational study of Smalley et al. (2024) uses a combination of geostationary and microwave imager data to find a strong diurnal cycle in the response of the domain mean LWP to variation in N_c. Decreases in LWP are observed during the day and neutral or positive responses of LWP during the night time hours. They

https://doi.org/10.5194/egusphere-2025-714
Preprint. Discussion started: 4 March 2025

speculated that this diurnal cycle in LWP sensitivity was driven primarily by the diurnal variation in precipitation sensitivity however there is no way to confirm or refute the causation with observations. The discovery of this large diurnal cycle in the cloud adjustments presents yet another significant uncertainty in our current knowledge because the ERF_{ACI} is weighted by the diurnally varying incoming solar radiation.

Many Large-Eddy Simulation (LES) studies use idealized scenarios with constant forcings to extract key controls of the system and simplify the interpretation of the results. This has generally been the case for the many studies examining aerosol indirect effects as well (e.g., Hoffmann et al., 2020). While this approach has the advantage of simplicity it neglects two important modes of variability in the subtropical cloudy boundary layer: (1) the large diurnal cycle, and (2) the multi-day transition of stratocumulus to cumulus boundary layers. A handful of studies have touched on these modes of variability in the context of aerosol indirect effects. For example, the study of Sandu et al. (2008) shows that increases in N_c increase the amplitude of the diurnal cycle of LWP_c in simulated stratocumulus. Furthermore, Sandu and Stevens (2011) show that transitions from Stratocumulus to Cumulus are a response to increasing Sea Surface Temperatures through Lagrangian LES in the North East Pacific. However, Yamaguchi et al. (2017) find that aerosol number concentration influences the timing of the transition through its mediation of drizzle. Prabhakaran et al. (2024) perform Lagrangian simulations of Stratocumulus perturbed by localized pulses of aerosol perturbations designed to simulate intentional marine cloud brightening. They find a distinct diurnal cycle in the cloud property sensitivity with negative cloud adjustments occurring in the afternoon and positive adjustments in the early morning, which they attribute to differences in absorbed solar radiation in the cloud layer. Erfani et al. (2022) perform Lagrangian LES along a subtropical cloud transition and demonstrate that the LWP adjustment depends on the cloud state, where the cloud adjustments are more pronounced along a pristine precipitating trajectory.

2 Methodology

2.1 Lagrangian Trajectory

The Lagrangian trajectory selected for this study was chosen from the many produced in Smalley et al. (2024) using the methodology outlined in Smalley et al. (2022). The trajectory is propagated forward in time using a 10 minute time step with the 3-hourly 925 hPa winds from the Modern-Era Retrospective analysis for Research and Applications, version 2 (MERRA-2 Gelaro et al., 2017). The selected trajectory west of Peru spans about 3800 km and extends from the subtropics to the tropics over the Pacific Ocean (Fig. 1). It represents a classical example of the stratocumulus-to-cumulus transition (SCT) for an air mass propagating over the ocean upon increasing sea surface temperature (SST) and reduced large-scale subsidence. It starts at 20^0S and 80^0W on 2019-10-06 00:00:00 UTC (i.e., around 18:00 local time) and follows the mean PBL flow during its six-day evolution. Note that the calculated trajectory provides only an approximate reconstruction of the real air mass movement due to both the presence of wind shear and the limited accuracy and resolution of reanalysis data.

Several observed cloud properties are matched to the trajectory where they are available. These include LWP from the fleet of passive microwave imagers (Wentz and Spencer, 1998). Higher frequency LWP observations are taken from the corrected geostationary data of Smalley and Lebsock (2023). Additional geostationary data products derived from the Advanced Base-

https://doi.org/10.5194/egusphere-2025-714
Preprint. Discussion started: 4 March 2025

line Imager (ABI) on GOES-16 include the cloud fraction, cloud top height, cloud optical depth, and cloud effective radius (Walther and Straka, 2019–2021). Finally, the profiles of several MERRA-2 variables are collocated along the trajectory to provide forcing data for the LES. These variables include horizontal wind components, water vapor, potential temperature, and large-scale subsidence, in addition to sea surface temperature.

2.2 Large-Eddy Simulations

We use the System for Atmospheric Modeling (Khairoutdinov and Randall, 2003) to simulate the transition. The domain size is 40.92×40.92 km^2. The horizontal grid spacing is 40 m, while the vertical grid spacing is 8 m in the PBL, gradually increasing with altitude. The initial and boundary conditions are based on MERRA-2 reanalysis data interpolated to the trajectory points. However, adjustments to the initial atmospheric state were necessary to reproduce the thick stratocumulus layer observed on that day. The most important change is sharpening the inversion layer to around 40 m instead of the original MERRA-2 resolution, which only produces shallow convection.

The free-tropospheric temperature and moisture profiles are nudged with 1-hr timescale starting 500-m above the PBL height defined as the top of inversion layer. Because the model cannot directly follow changes in the mesoscale pressure gradient that controls boundary-layer winds, we apply weak nudging of the mean PBL winds with a timescale of 12 hours. Furthermore, to suppress the development of spurious circulations within the domain during longer simulations, we apply weak homogenization with a 48-hour timescale. Microphysics is parameterized using the one-moment scheme of Khairoutdinov and Kogan (2000), and four different aerosol-related scenarios are prescribed along the trajectory in terms of droplet number concentrations (Fig. 1). All scenarios begin with high coastal droplet number concentrations typical of polluted continental air, gradually decreasing to 25 cc^{-1} for pristine air, 50 cc^{-1} and 100 cc^{-1} for intermediate conditions, and 200 cc^{-1} for polluted air. These scenarios represent the uncertainty in aerosol-cloud interactions and their impact on cloud microphysics and radiative properties, as well as observational uncertainties. The sea surface temperature changes from approximately 290 K to nearly 297 K, with surface fluxes interactively calculated based on local atmospheric conditions near the surface. Interactive short-wave and long-wave radiation effects are also included. A similar Lagrangian perspective and modeling setup was applied in many other studies (e.g., van der Dussen et al., 2013; Sandu and Stevens, 2011; Yamaguchi et al., 2017). Note that while the boundary conditions follow observations, the PBL development is determined by the processes occurring within it.

2.3 Diurnal Controls of Indirect Radiative Effect

To understand the relative diurnal contributions of the Twomey effect and the cloud adjustments to the indirect effect, offline radiative transfer calculations are performed. The reflected shortwave flux is given by

$$F^{\uparrow} = F_o \mu_o A \tag{2}$$

where F_o is the solar constant, μ_o is the cosine of the solar zenith angle, and A is the all-sky albedo. The all-sky albedo is calculated as the sum of a clear and cloud sky components

$$A = (1 - f_c)\alpha_{surf} + f_c A_c \tag{3}$$

https://doi.org/10.5194/egusphere-2025-714
Preprint. Discussion started: 4 March 2025

where α_{surf} is the ocean surface albedo assumed to be 0.06, and A_{cld} is the albedo of the cloudy part of the domain. Accounting for multiple reflections between a cloud layer with albedo (α_{cld}) and the reflecting surface this is

$$A_c = \alpha_{cld} + \frac{\alpha_{surf}(1-\alpha_{cld})^2}{1-\alpha_{surf}\alpha_{cld}} \tag{4}$$

Appendix A describes the offline calculations of α_{cld}, including a proper accounting of the solar zenith angle, which is a critical factor when addressing the diurnal cycle. Finally, the Cloud Radiative Effect (*CRE*) is calculated as

$$CRE = F_o \mu_o f_c (A_{cld} - \alpha_{srf}) \tag{5}$$

The cloud optical depth is calculated at each time step from the domain mean time-dependent modeled LWP_c and N_c assuming an adiabatic cloud vertical structure following Hoffmann et al. (2023)

$$\tau_c = 0.2\, {N_c}^{1/3} {LWP_c}^{5/6} \tag{6}$$

The offline radiation calculations are used to decompose the $\mathrm{ERF_{ACI}}$ into the three indirect sensitivity terms. Knowing that $F^{\uparrow} = F^{\uparrow}(N_c, LWP_c, f_c)$, the sensitivity can be estimated using the pristine and polluted simulation results as follows:

$$S_N = \left.\frac{d\ln F^{\uparrow}}{d\ln N_c}\right|_{\overline{\mathrm{LWP}_c},\overline{f_c}} = \frac{\ln F^{\uparrow}(N_{c200}, \overline{\mathrm{LWP}_c}, \overline{f_c}) - \ln F^{\uparrow}(N_{c25}, \overline{\mathrm{LWP}_c}, \overline{f_c})}{\ln N_{c200} - \ln N_{c25}} \tag{7}$$

$$S_{\mathrm{LWP}} = \left.\frac{d\ln F^{\uparrow}}{d\ln N_c}\right|_{\overline{N_c},\overline{f_c}} = \frac{\ln F^{\uparrow}(\overline{N_c}, \overline{\mathrm{LWP}}_c(N_{c200}), \overline{f_c}) - \ln F^{\uparrow}(\overline{N_c}, \overline{\mathrm{LWP}}_c(N_{c25}), \overline{f_c})}{\ln N_{c200} - \ln N_{c25}} \tag{8}$$

$$S_f = \left.\frac{d\ln F^{\uparrow}}{d\ln N_c}\right|_{\overline{N_c},\overline{\mathrm{LWP}_c}} = \frac{\ln F^{\uparrow}(\overline{N_c}, \overline{\mathrm{LWP}}_c, \overline{f_c}(N_{c200})) - \ln F^{\uparrow}(\overline{N_c}, \overline{\mathrm{LWP}}_c, \overline{f_c}(N_{c25}))}{\ln N_{c200} - \ln N_{c25}} \tag{9}$$

Here, the overbar represents the mean of the polluted and pristine simulations along the trajectory, meaning that for each of the three terms, we estimate the sensitivity of $F^{\uparrow}$ in only one direction within the three-dimensional parameter space, while keeping the other two parameters fixed at their mean values. Note that, because these sensitivities are expressed in terms of reflected fluxes rather than albedo, they account for the diurnal variation in incoming solar flux. Furthermore, since we analyze the susceptibility of $\ln F^{\uparrow}$ rather than $F^{\uparrow}$ itself, the results are intended to be more universal across seasons, as they are scaled by solar insolation.

2.4 Results

2.4.1 Evaluation of LES evolution against observations

We begin by evaluating the diurnal evolution of the simulated clouds and the realism of the LES against the observations. Figure 1 provides a summary of the evolution of the clouds for four N_c scenarios over the six-day simulation. Panel a shows

https://doi.org/10.5194/egusphere-2025-714
Preprint. Discussion started: 4 March 2025

the path of the trajectory while panel f shows the Sea Surface Temperature (SST) along the trajectory. Panel e shows the imposed number concentrations, loosely based on observations from the ABI, which begins at large values of several hundred cm^{-3} near the coast and asymptotes to values ranging between 25 and 200 cm^{-3} in the tropics. Most of this paper will contrast the pristine (25 cm^{-3}) simulation with the polluted (200 cm^{-3}) simulation. Panel h shows the expected increases in τ_c with increases in N_c. Panels d (polluted) and i (pristine) highlight two critical features of the simulations. First, the polluted cloud grows significantly deeper than the pristine cloud and that growth occurs in the overnight and early morning hours. Second, the pristine cloud produces substantially more drizzle than the polluted clouds. Each of these observations is consistent with expectations that increasing N_c should both suppress precipitation and increase the cloud top entrainment efficiency. Next, note that the diurnal evolution of the LWP and f_c (panels b, g) show general agreement with the observations, while differing in some of the precise details. For example, the LES is not able to produce sufficiently thick and extensive cloud cover over the nighttime hours of days 2-4. We also note that the pristine experiment, which is the most realistic scenario, is well able to simulate the observed cloud top height (CTH), whereas the more polluted experiments show larger growth of the cloud layer (panel c), which is not observed in this case but remains a physically plausible outcome under different conditions.

2.4.2 Cloud Radiative Effects

How does the distinct diurnal variation in cloud properties affect the ERF_{ACI}? Figure 2 contrasts the pristine and polluted scenarios to understand the relative influence of cloud adjustments relative to the Twomey effect on the CRE. The largest differences in LWP_c occur during the overnight and early morning hours due to the suppression of precipitation (panel a). In contrast, during mid-day, the polluted LWP_c is smaller than the pristine scenario. The f_c adjustment follows a similar diurnal pattern, with the polluted scenario showing a larger f_c overnight into the morning, and a smaller f_c in the afternoon (panel b). Panel c compares the cloud albedo of the pristine and polluted scenarios, including both the Twomey effect and the LWP adjustment. The polluted A_c is generally larger than the pristine, except for a few hours during midday when the reductions in LWP_c more than offset the Twomey effect brightening. What ultimately matters for the energy budget of the system is the CRE shown in panel d. Here, a distinct diurnal pattern emerges in the difference between the polluted and pristine scenarios. In the polluted scenario, there is a distinct increase in CRE in the morning, while in the early afternoon, there are modest decreases. Occasionally, a secondary increase in CRE occurs in the evening when the cloud layer is recovering from its afternoon minimum.

It is important to recognize that two factors limit the sensitivity of CRE to N_c at large solar zenith angle. First, the incoming solar flux scales as μ_o and second as the cloud albedo approaches unity the Twomey effect tends to zero. As a result, the fairly large cloud adjustment terms in the early morning hours are not very effective at increasing the diurnal average CRE.

Figure 3 shows a composite diurnal cycle of the ERF_{ACI} averaged over the six-day trajectory. Here panel a shows the three individual terms that determine the ERF_{ACI}. The Twomey effect (S_N) is always positive with a peak in the late morning. The timing of this peak in S_N results from a combination of the fact that sensitivity is maximum for $A_c = 0.5$ (Platnick and Twomey, 1994) and of the fact that morning hours have larger f_c than afternoon hours, so that the Twomey effect has less leverage in the afternoon than in the morning. The cloud adjustment terms (S_{LWP}, S_f) have similar patterns with positive/negative

https://doi.org/10.5194/egusphere-2025-714
Preprint. Discussion started: 4 March 2025

values in the morning/afternoon that mediate the Twomey effect. Panel b shows the total ERF_{ACI}, which is largely positive in the morning and approximately zero in the afternoon. Overall, the cloud adjustments are approximately zero over the diurnal average, acting to enhance the Twomey effect in the morning and nearly cancel it in the afternoon. The daylight averages of the three terms are $S_N = 0.0068$, $S_{LWP} = -0.0025$, $S_f = 0.0019$.

2.4.3 Role of Key Physical Processes/ Key Controls

Why does the diurnal pattern in ERF_{ACI} seen in Figure 3 emerge? To demonstrate the relevant mechanisms, Figure 4 presents a composite diurnal comparison of the cloudy boundary layer structure for the pristine and polluted scenarios. The polluted scenario produces less precipitation than the pristine scenario at all hours of the day (panel a). The polluted cloud entrains more efficiently and grows deeper than the pristine cloud over night (panel b). The polluted cloud is substantially more turbulent than the pristine cloud over night (panel e). Panel d shows that while the changes in cloud LWP affect the radiative heating of the cloud layer, the afternoon differences in the shortwave warming are nearly exactly canceled by the differences in the longwave cooling. The resultant difference in radiative heating is primarily due to an overnight increases in longwave cooling of the polluted case. While both clouds are well coupled to the surface fluxes over night, the polluted cloud becomes substantially less coupled than the pristine cloud throughout the sunlit hours (Panel c). The decoupling index is defined here as the ratio of the cloud base flux to the near-surface flux (van der Dussen et al., 2013).

Overall, a picture emerges of a polluted cloud that grows substantially faster over night than the pristine cloud with enhanced LWP due to precipitation suppression and a deeper cloud layer. However, this enhanced growth of the polluted cloud results in a deeper boundary layer that is more easily decoupled from the surface fluxes during the afternoon hours. These results explain the consistently positive (early morning) and negative (afternoon) sensitivities seen in Figures 2 and 3.

In our experimental design, modifying N_c influences three model processes directly: radiative transfer, autoconversion, and cloud water sedimentation. We perform a series of additional experiments where we impose the polluted N_c on a particular process rate while all other processes see the pristine N_c to demonstrate the importance of that process on the evolution of the boundary layer and cloud macrophyscial properties. We show the evolution of four quantities to demonstrate the influence of the various processes. The first two are cloud macrophysical quantities: LWP and rain water path (RWP). The second two are related to the structure of the boundary layer: inversion height z_{inv} and decoupling index. Figure 5 shows the evolution of these four quantities for the various experiments. Several conclusions can be formed from these results:

- The influence of N_c on radiative transfer has a marginal effect on the evolution of the cloudy boundary layer. This is shown by the similarity between Exp. 3 and the pristine scenario (panels a-d).
- The autoconversion process has a positive and distinctly diurnal influence on the LWP sensitivity, while the cloud water sedimentation process has a smaller, negative, and relatively constant influence (panel e).
- Both autoconversion and, to a lesser extent, cloud water sedimentation affect the precipitation suppression mechanism (panel f). The latter process indirectly influences rainwater production by removing cloud liquid from the cloud top, thus limiting the efficiency of autoconversion.

https://doi.org/10.5194/egusphere-2025-714
Preprint. Discussion started: 4 March 2025

– Both autoconversion and cloud water sedimentation influence the entrainment efficiency and growth of the boundary layer. Autoconversion has a larger effect than cloud water sedimentation, and the two processes interact in a super-linear manner to influence entrainment efficiency (panel g).

– Both autoconversion and cloud water sedimentation contribute to the decoupling of the cloud layer from the surface (panel h), which is consistent with the fact that both processes individually affect the cloud top entrainment rate.

A key summary of these conclusions is that the autoconversion and the cloud water sedimentation processes have some similar influences on the development of the cloudy boundary layer. The reason for this is that both processes remove liquid from the cloud top entrainment zone, thereby slowing the rate of precipitation production, decreasing the efficiency of the entrainment, and slowing the decoupling of the boundary layer. This is closely related to the dynamics of the Entrainment Interfacial Layer (EIL; Haman et al., 2007; Kurowski et al., 2009), where the removal of liquid from the cloud top influences the structure of the EIL, leading to changes in boundary layer growth. We also see that these processes interact in a non-linear way, particularly in their influence on the LWP and the entrainment rate. Furthermore, the strong diurnal cycle in the sensitivity of cloud properties is a result primarily of the autoconversion process, whereas the cloud water sedimentation process operates over a longer time scale.

3 Conclusions

This paper shows the results of a six-day Lagrangian LES along the stratocumulus to cumulus transition with realistic environmental forcing including a diurnal cycle of solar radiation. Pristine and polluted scenarios are simulated to quantify the $\mathrm{ERF_{ACI}}$ and its component terms. The $\mathrm{ERF_{ACI}}$ is broken down into the Twomey effect, a $\mathrm{LWP_c}$ adjustment, and a f_c adjustment. The daytime average values of the three terms are 0.0068, -0.0025, 0.0019, respectively. However, there is a susbstantial diurnal cycle in the three terms. The Twomey effect is always positive and most efficient in the morning hours because the f_c is larger in the morning than the afternoon. More significantly, the $\mathrm{LWP_c}$ and f_c adjustments switch signs from positive to negative from morning into the afternoon. The resultant diurnal pattern of the $\mathrm{ERF_{ACI}}$ is super-Twomey in the morning and near neutral in the afternoon.

The reason this pattern in $\mathrm{ERF_{ACI}}$ emerges is that the diurnal amplitude of the cloud macrophysical properties is increased relative to the pristine case. This occurs because precipitation is suppressed in the polluted cloud relative to the pristine resulting in a thicker more turbulent cloud, with enhanced longwave cooling and increased cloud liquid water near the cloud top entrainment zone during the nighttime hours. As a result of the increase cloud top liquid water the polluted cloud entrains more efficiently and grows substantially faster and deeper overnight. However this nighttime success of the polluted cloud is not sustainable as it results in a boundary layer that is deeper, drier and more decoupled, which ultimately leads to a stronger mid-day collapse of the cloudy boundary layer the following afternoon.

A key mechanism in the causal chain is the increase in cloud top liquid water with increases in N_c. Through sensitivity experiments it is shown that both sedimentation of cloud and rain water are effective at reducing the efficiency of the entrainment.

https://doi.org/10.5194/egusphere-2025-714
Preprint. Discussion started: 4 March 2025

However, cloud sedimentation and autoconversion interact in a nonlinear manner to result in a combined effect on entrainment that is greater than the sum of each term. This could occur due to the non-linearity of the autoconversion process interacting with a reduced amount of cloud liquid water at cloud top due to the cloud water sedimentation. Therefore, accurate simulation of the entrainment drying mechanism in global models should include both cloud and rain water sedimentation as is the case in at least one commonly used cloud microphysics parameterization (Morrison and Gettelman, 2008).

The findings of this study are in qualitative agreement with a growing body of literature based on both modeling and observations that increasing N_c causes an amplification of the diurnal cycle of cloud properties which subsequently causes a morning/afternoon contrast in the sign of the cloud adjustments with adjustments enhancing Twomey brightening in the morning and offsetting the brightening in the afternoon. The result in this study is a negligible diurnal average effect of the adjustments on the ERF_{ACI}. However, this is based on a single suite of simulations and we must be cautious in extrapolating these results to more general conditions. In particular, a key mechanism that mediates the diurnal response in these simulations is the suppression of precipitation. We have no expectations that increasing in N_c in non-precipitating clouds would have the same effect on the diurnal cycle. We could speculate that in that case the cloud adjustments would be robustly negative across the diurnal cycle. Future research is necessary to extend the Lagrangian approach used here to many more trajectories representative of the diversity of atmospheric conditions to fully understand the influence of the diurnal cycle of the cloud adjustments on the ERF_{ACI}.

Code availability. The System for Atmospheric Modeling code is available upon contacting Dr. Marat Khairoutdinov

Data availability. Trajectory data, model inputs and outputs needed to reproduce the figures are avaliable at: https://zenodo.org/records/14873449

Appendix A

The cloud albedo is calculated using the hybrid model of Meador and Weaver (1980), which includes a dependence on the solar zenith angle.

$$\alpha_{cld} = \frac{1}{1+\gamma_1\tau_c}\left(\gamma_1\tau_c + (\beta_o - \gamma_1\mu_o)\left(1 - \exp\left(\frac{-\tau_c}{\mu_0}\right)\right)\right) \tag{A1}$$

The two γ coefficients of this model are given by

$$\gamma_1 = \frac{7-3g^2-\omega_o(4+3g)+\omega_o g^2(4\beta_o+3g)}{4(1-g^2(1-\mu_0))} \tag{A2}$$

$$\gamma_2 = \frac{1-g^2-\omega_o(4+3g)-\omega_o g^2(4\beta_o+3g-4)}{-4(1-g^2(1-\mu_0))} \tag{A3}$$

where ω_o is the single scatter albedo and g is the asymetery parameter. The third coefficient is given by

$$\beta_o = \frac{1}{2\omega_o}\int_0^1 P(\mu_o, -\mu')\, d\mu' \tag{A4}$$

https://doi.org/10.5194/egusphere-2025-714
Preprint. Discussion started: 4 March 2025

which is the the fraction of single scattered radiation out of the solar beam into the backscattering hemisphere. The single scattering phase function (P) is subject to the normalization condition

$$\frac{1}{4\pi}\int_{-1}^{1}\int_{0}^{2\pi} P(\mu,\phi;\mu',\phi')\,d\phi' d\mu' = \omega_o \tag{A5}$$

The inclusion of the β_o term is a complication as in general it represents an integral that can not be represented analytically. In this work, we parameterize this integral based on numerical integration of the Henyey and Greenstein (1941) phase function for $g = 0.86$ and $\omega_o = 1$ giving the follow approximate formulation

$$\beta_o(g = 0.86, \omega_o = 1) \approx 0.5 \exp -2.7\mu_o^{0.7} \tag{A6}$$

where the Henyey-Greenstein phase function subject to the proper normalization is given by

$$P_{HG} = \omega_o \frac{1-g^2}{(1+g^2-2gcos(\Theta))^{\frac{3}{2}}} \tag{A7}$$

Author contributions. MK and ML designed the experiments and MK carried them out. KS prepared the Lagrangian trajectory and observational data. MK developed the model code and performed the simulations. MK and ML preformed the analysis. MK prepared the manuscript with contributions from all co-authors.

Competing interests. At least one of the (co-)authors is a member of the editorial board of *Atmospheric Chemistry and Physics.*

Acknowledgements. The research was carried out at the Jet Propulsion Laboratory, California Institute of Technology, under a contract with the National Aeronautics and Space Administration (80NM0018D0004). Texas Advanced Computing Center (TACC) The University of Texas at Austin is acknowledged for providing high-performance computing resources. Work from LLNL is performed under the auspices of the US DOE by LLNL under Contract DE-AC52-07NA27344: IM Number LLNL-ABS-867332. LLNL-JRNL-2002664.

https://doi.org/10.5194/egusphere-2025-714
Preprint. Discussion started: 4 March 2025

References

Ackerman, A. S., Toon, O. B., Stevens, D. E., Heymsfield, A. J., Ramanathan, V., and Welton, E. J.: Reduction of tropical cloudiness by soot, Science, 288, 1042–1047, https://doi.org/10.1126/science.288.5468.1042, 2000.

Ackerman, A. S., Kirkpatrick, M. P., Stevens, D. E., and Toon, O. B.: The impact of humidity above stratiform clouds on indirect aerosol climate forcing, Nature, 432, 1014–1017, https://doi.org/10.1038/nature03174, 2004.

Albrecht, B. A.: Aerosols, Cloud Microphysics, and Fractional Cloudiness, Science, 245, 1227–1230, 1989.

Bellouin, N., Quaas, J., Gryspeerdt, E., Kinne, S., Stier, P., Watson-Parris, D., Boucher, O., Carslaw, K. S., Christensen, M., Daniau, A.-L., Dufresne, J.-L., Feingold, G., Fiedler, S., Forster, P., Gettelman, A., Haywood, J. M., Lohmann, U., Malavelle, F., Mauritsen, T., McCoy, D. T., Myhre, G., Mülmenstädt, J., Neubauer, D., Possner, A., Rugenstein, M., Sato, Y., Schulz, M., Schwartz, S. E., Sourdeval, O., Storelvmo, T., Toll, V., Winker, D., and Stevens, B.: Bounding Global Aerosol Radiative Forcing of Climate Change, Reviews of Geophysics, 58, e2019RG000 660, 2020.

Bretherton, C. S., Blossey, P. N., and Uchida, J.: Cloud droplet sedimentation, entrainment efficiency, and subtropical stratocumulus albedo, Geophysical Research Letters, 34, 2007.

Christensen, M. W. and Stephens, G. L.: Microphysical and macrophysical responses of marine stratocumulus polluted by underlying ships: 2. Impacts of haze on precipitating clouds, Journal of Geophysical Research: Atmospheres, 117, 2012.

Christensen, M. W., Neubauer, D., Poulsen, C. A., Thomas, G. E., McGarragh, G. R., Povey, A. C., Proud, S. R., and Grainger, R. G.: Unveiling aerosol–cloud interactions – Part 1: Cloud contamination in satellite products enhances the aerosol indirect forcing estimate, Atmospheric Chemistry and Physics, 17, 13 151–13 164, 2017.

Coakley, J. A. and Walsh, C. D.: Limits to the Aerosol Indirect Radiative Effect Derived from Observations of Ship Tracks, Journal of the Atmospheric Sciences, 59, 668 – 680, 2002.

Diamond, M. S., Director, H. M., Eastman, R., Possner, A., and Wood, R.: Substantial Cloud Brightening From Shipping in Subtropical Low Clouds, AGU Advances, 1, e2019AV000 111, 2020.

Erfani, E., Blossey, P., Wood, R., Mohrmann, J., Doherty, S. J., Wyant, M., and O, K.-T.: Simulating Aerosol Lifecycle Impacts on the Subtropical Stratocumulus-to-Cumulus Transition Using Large-Eddy Simulations, Journal of Geophysical Research: Atmospheres, 127, e2022JD037 258, 2022.

Gelaro, R., McCarty, W., Suárez, M. J., Todling, R., Molod, A., Takacs, L., Randles, C. A., Darmenov, A., Bosilovich, M. G., Reichle, R., Wargan, K., Coy, L., Cullather, R., Draper, C., Akella, S., Buchard, V., Conaty, A., da Silva, A. M., Gu, W., Kim, G.-K., Koster, R., Lucchesi, R., Merkova, D., Nielsen, J. E., Partyka, G., Pawson, S., Putman, W., Rienecker, M., Schubert, S. D., Sienkiewicz, M., and Zhao, B.: The Modern-Era Retrospective Analysis for Research and Applications, Version 2 (MERRA-2), Journal of Climate, 30, 5419 – 5454, 2017.

Gryspeerdt, E., Quaas, J., and Bellouin, N.: Constraining the aerosol influence on cloud fraction, Journal of Geophysical Research: Atmospheres, 121, 3566–3583, 2016.

Haman, K. E., Malinowski, S. P., Kurowski, M. J., Gerber, H., and Brenguier, J.-L.: Small scale mixing processes at the top of a marine stratocumulus—a case study, Quarterly Journal of the Royal Meteorological Society, 133, 213–226, 2007.

Han, Q., Rossow, W. B., Zeng, J., and Welch, R.: Three Different Behaviors of Liquid Water Path of Water Clouds in Aerosol–Cloud Interactions, Journal of the Atmospheric Sciences, 59, 726 – 735, 2002.

Henyey, L. G. and Greenstein, J. L.: Diffuse radiation in the galaxy, Astrophysical Journal, 93, 70–83, https://doi.org/10.1086/144246, 1941.

https://doi.org/10.5194/egusphere-2025-714
Preprint. Discussion started: 4 March 2025

Hoffmann, F., Glassmeier, F., Yamaguchi, T., and Feingold, G.: Liquid Water Path Steady States in Stratocumulus: Insights from Process-Level Emulation and Mixed-Layer Theory, Journal of the Atmospheric Sciences, 77, 2203 – 2215, 2020.

Hoffmann, F., Glassmeier, F., Yamaguchi, T., and Feingold, G.: On the Roles of Precipitation and Entrainment in Stratocumulus Transitions between Mesoscale States, Journal of the Atmospheric Sciences, 80, 2791–2803, https://doi.org/10.1175/JAS-D-22-0268.1, 2023.

IPCC: Climate Change 2021: The Physical Science Basis. Contribution of Working Group I to the Sixth Assessment Report of the Intergovernmental Panel on Climate Change, Cambridge University Press, Cambridge, UK and New York, NY, USA, https://doi.org/10.1017/9781009157896, 2021.

IPCC: Climate Change 2022: Mitigation of Climate Change. Contribution of Working Group III to the Sixth Assessment Report of the Intergovernmental Panel on Climate Change, Cambridge University Press, Cambridge, UK and New York, NY, USA, https://doi.org/10.1017/9781009157926, 2022.

Khairoutdinov, M. and Kogan, Y.: A New Cloud Physics Parameterization in a Large-Eddy Simulation Model of Marine Stratocumulus, Monthly Weather Review, 128, 229 – 243, 2000.

Khairoutdinov, M. F. and Randall, D. A.: Cloud Resolving Modeling of the ARM Summer 1997 IOP: Model Formulation, Results, Uncertainties, and Sensitivities, Journal of the Atmospheric Sciences, 60, 607 – 625, 2003.

Kurowski, M. J., P. Malinowski, S., and W. Grabowski, W.: A numerical investigation of entrainment and transport within a stratocumulus-topped boundary layer, Quarterly Journal of the Royal Meteorological Society, 135, 77–92, 2009.

Lebsock, M. D., Stephens, G. L., and Kummerow, C.: Multisensor satellite observations of aerosol effects on warm clouds, Journal of Geophysical Research: Atmospheres, 113, 2008.

Manshausen, P., Watson-Parris, D., Christensen, M. W., Stier, P., Neubauer, D., and Grosvenor, D. P.: Invisible ship tracks show large cloud sensitivity to aerosol, Nature, 610, 101–106, https://doi.org/10.1038/s41586-022-05122-0, 2022.

Meador, W. E. and Weaver, W. R.: Two-Stream Approximations to Radiative Transfer in Planetary Atmospheres: A Unified Description of Existing Methods and a New Improvement, Journal of Atmospheric Sciences, 37, 630 – 643, 1980.

Morrison, H. and Gettelman, A.: A New Two-Moment Bulk Stratiform Cloud Microphysics Scheme in the Community Atmosphere Model, Version 3 (CAM3). Part I: Description and Numerical Tests, Journal of Climate, 21, 3642 – 3659, 2008.

Pincus, R. and Baker, M.: Effect of precipitation on the albedo susceptibility of clouds in the marine boundary layer, Nature, 372, 250–252, https://doi.org/10.1038/372250a0, 1994.

Platnick, S. and Twomey, S.: Determining the Susceptibility of Cloud Albedo to Changes in Droplet Concentration with the Advanced Very High Resolution Radiometer, Journal of Applied Meteorology and Climatology, 33, 334 – 347, 1994.

Prabhakaran, P., Hoffmann, F., and Feingold, G.: Effects of intermittent aerosol forcing on the stratocumulus-to-cumulus transition, Atmospheric Chemistry and Physics, 24, 1919–1937, 2024.

Quaas, J., Arola, A., Cairns, B., Christensen, M., Deneke, H., Ekman, A. M. L., Feingold, G., Fridlind, A., Gryspeerdt, E., Hasekamp, O., Li, Z., Lipponen, A., Ma, P.-L., Mülmenstädt, J., Nenes, A., Penner, J. E., Rosenfeld, D., Schrödner, R., Sinclair, K., Sourdeval, O., Stier, P., Tesche, M., van Diedenhoven, B., and Wendisch, M.: Constraining the Twomey effect from satellite observations: issues and perspectives, Atmospheric Chemistry and Physics, 20, 15 079–15 099, 2020.

Sandu, I. and Stevens, B.: On the Factors Modulating the Stratocumulus to Cumulus Transitions, Journal of the Atmospheric Sciences, 68, 1865 – 1881, 2011.

Sandu, I., Brenguier, J.-L., Geoffroy, O., Thouron, O., and Masson, V.: Aerosol Impacts on the Diurnal Cycle of Marine Stratocumulus, Journal of the Atmospheric Sciences, 65, 2705 – 2718, 2008.

https://doi.org/10.5194/egusphere-2025-714
Preprint. Discussion started: 4 March 2025

Smalley, K. M. and Lebsock, M. D.: Corrections for Geostationary Cloud Liquid Water Path Using Microwave Imagery, Journal of Atmospheric and Oceanic Technology, 40, 1049 – 1061, 2023.

Smalley, K. M., Lebsock, M. D., Eastman, R., Smalley, M., and Witte, M. K.: A Lagrangian analysis of pockets of open cells over the southeastern Pacific, Atmospheric Chemistry and Physics, 22, 8197–8219, 2022.

Smalley, K. M., Lebsock, M. D., and Eastman, R.: Diurnal Patterns in the Observed Cloud Liquid Water Path Response to Droplet Number Perturbations, Geophysical Research Letters, 51, e2023GL107 323, 2024.

Toll, V., Christensen, M., Quaas, J., and Bellouin, N.: Weak average liquid-cloud-water response to anthropogenic aerosols, Nature, 572, 51–55, https://doi.org/10.1038/s41586-019-1423-9, 2019.

Twomey, S.: The Influence of Pollution on the Shortwave Albedo of Clouds, Journal of Atmospheric Sciences, 34, 1149 – 1152, 1977.

van der Dussen, J. J., de Roode, S. R., Ackerman, A. S., Blossey, P. N., Bretherton, C. S., Kurowski, M. J., Lock, A. P., Neggers, R. A. J., Sandu, I., and Siebesma, A. P.: The GASS/EUCLIPSE model intercomparison of the stratocumulus transition as observed during ASTEX: LES results, Journal of Advances in Modeling Earth Systems, 5, 483–499, 2013.

Várnai, T. and Marshak, A.: MODIS observations of enhanced clear sky reflectance near clouds, Geophysical Research Letters, 36, 2009.

Wall, C. J., Norris, J. R., Possner, A., McCoy, D. T., McCoy, I. L., and Lutsko, N. J.: Assessing effective radiative forcing from aerosol–cloud interactions over the global ocean, Proceedings of the National Academy of Sciences, 119, e2210481 119, 2022.

Wall, C. J., Storelvmo, T., and Possner, A.: Global observations of aerosol indirect effects from marine liquid clouds, Atmospheric Chemistry and Physics, 23, 13 125–13 141, 2023.

Walther, A. and Straka, W.: Cloud optical depth from the National Oceanic and Atmospheric Administration (NOAA) comprehensive large array-data stewardship system (CLASS) [Dataset], retrieved from https://www.avl.class.noaa.gov/saa/products/search?sub_id=0&datatype_family=GRABIPRD&submit.x=20&submit.y=10, 2019–2021.

Wentz, F. J. and Spencer, R. W.: SSM/I Rain Retrievals within a Unified All-Weather Ocean Algorithm, Journal of the Atmospheric Sciences, 55, 1613 – 1627, 1998.

Yamaguchi, T., Feingold, G., and Kazil, J.: Stratocumulus to Cumulus Transition by Drizzle, Journal of Advances in Modeling Earth Systems, 9, 2333–2349, 2017.

https://doi.org/10.5194/egusphere-2025-714
Preprint. Discussion started: 4 March 2025

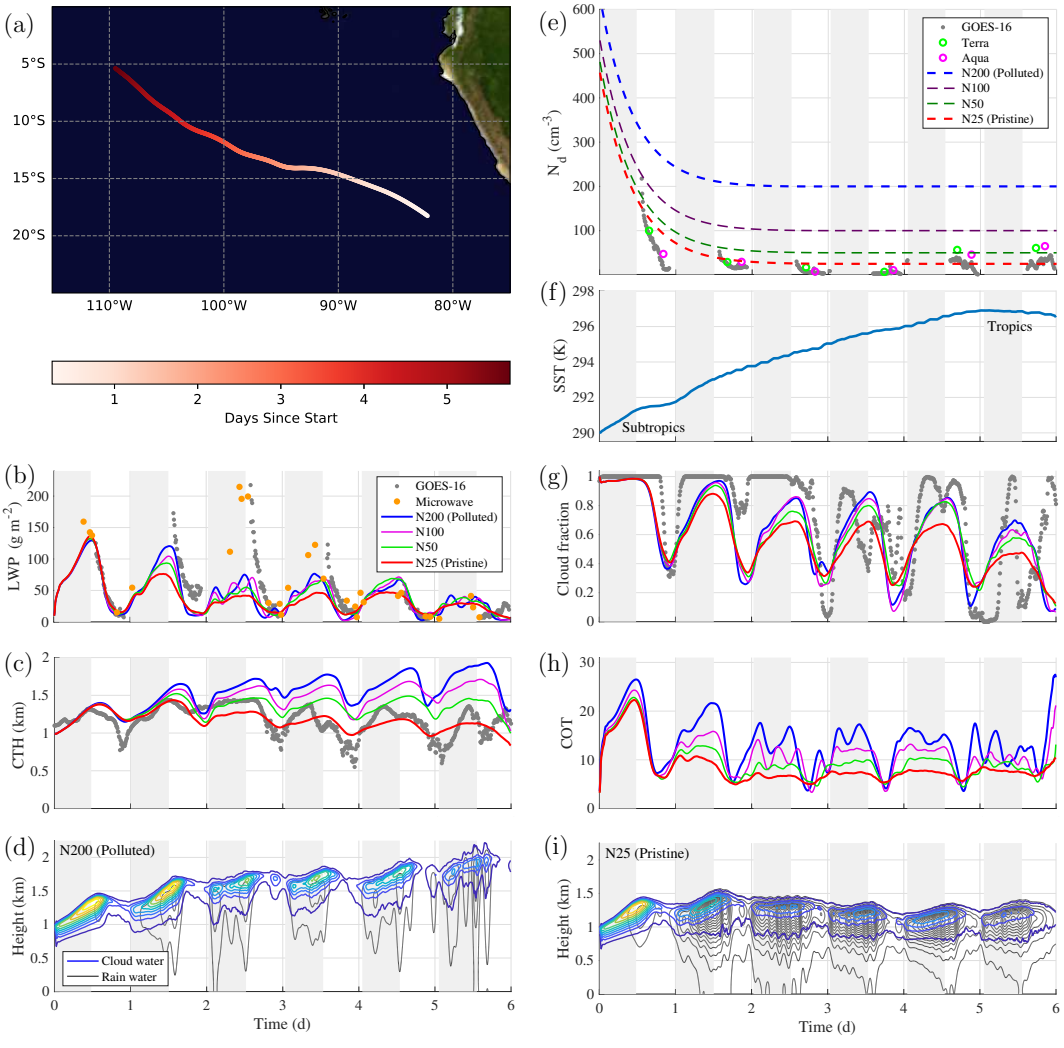

Figure 1. Overview of the analyzed case: (a) Lagrangian trajectory, and the evolution of (b) liquid water path from LES and observations, (c) cloud top height from LES and observations, (d) curtain plot of cloud water and rain water mixing ratios for the polluted case (N200), (e) observed and prescribed in LES droplet number concentrations, (f) sea surface temperature (SST), (g) observed and simulated cloud fraction, (h) cloud optical thickness from the LESs, (i) curtain plot of cloud water and rain water mixing ratios for the pristine case (N25).

https://doi.org/10.5194/egusphere-2025-714
Preprint. Discussion started: 4 March 2025

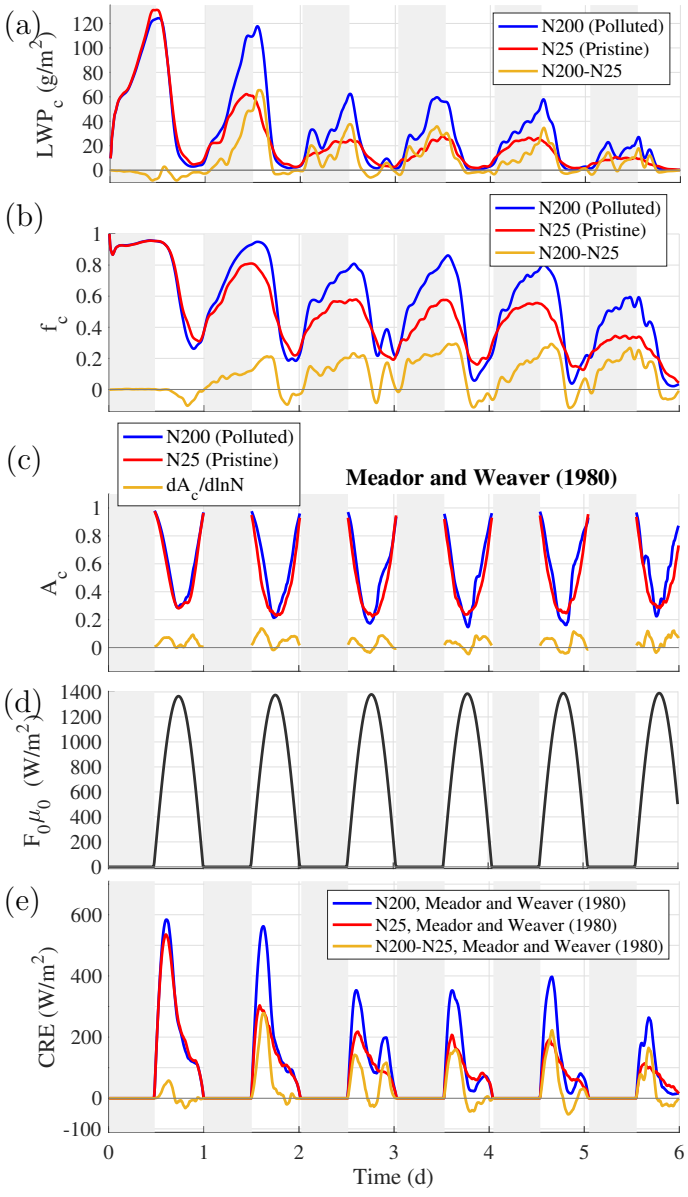

Figure 2. Six diurnal cycles of (a) cloud fraction and its difference between the polluted and pristine cases, (b) cloud albedo calculated following Meador and Weaver (1980) and its difference between the extreme cases, also compared to Twomey effect, and (c) cloud radiative effect along with its difference between the Polluted and Pristine cases. Twomey effect plotted in (b) is calculated as the difference between two values of cloud albedo calculated for the same cloud fraction f_c using two droplet number concentrations (i.e., pristine and polluted), and averaged over different cloud fractions.

https://doi.org/10.5194/egusphere-2025-714
Preprint. Discussion started: 4 March 2025

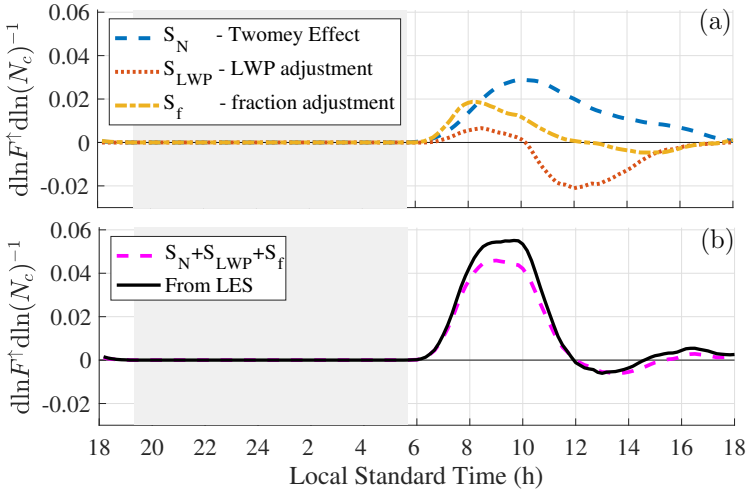

Figure 3. Composite diurnal cycle of: (a) the sensitivity terms S_N, S_{LWP}, S_f from Eqs. 7-9, calculated offline using the differences between the N200 and N25 simulations, and (b) their sum (magenta) compared against the actual LES model output (black).

https://doi.org/10.5194/egusphere-2025-714
Preprint. Discussion started: 4 March 2025

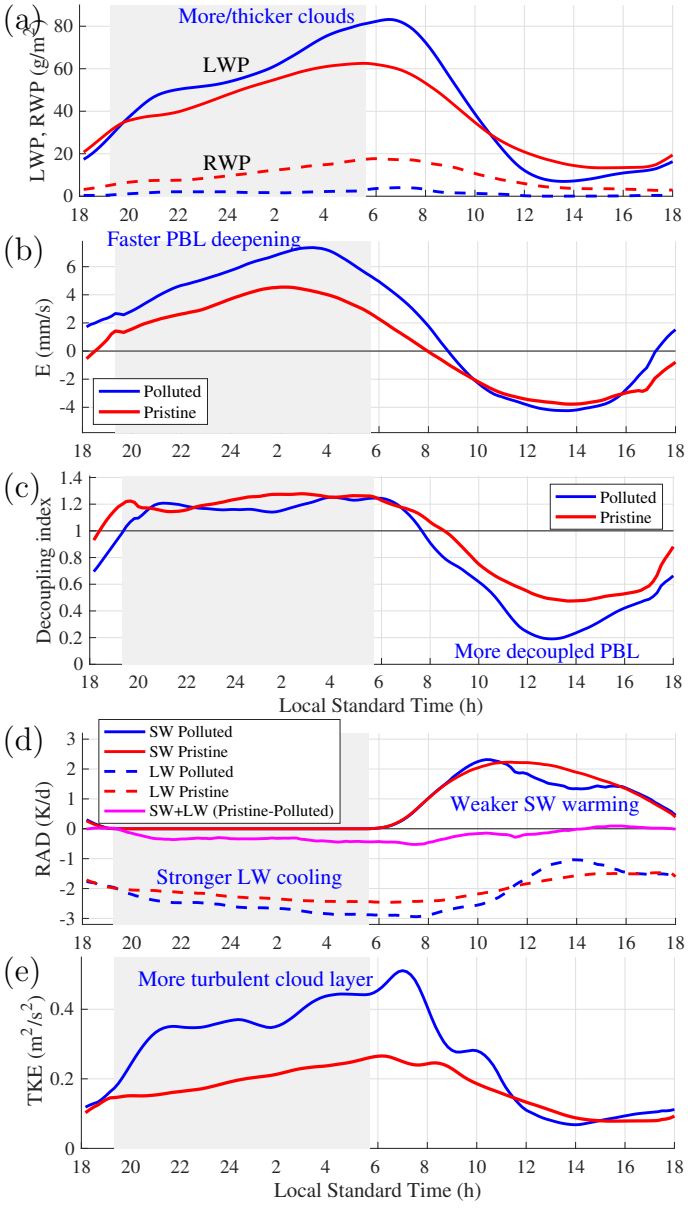

Figure 4. Composite diurnal cycle for the Pristine (red) and Polluted (blue) cases in terms of (a) LWP and RWP, (b) cloud-top entrainment rate, (c) PBL decoupling index, (d) cloud-layer SW and LW radiative tendencies and their total differences (magenta). Text in blue highlights the Polluted case.

https://doi.org/10.5194/egusphere-2025-714
Preprint. Discussion started: 4 March 2025

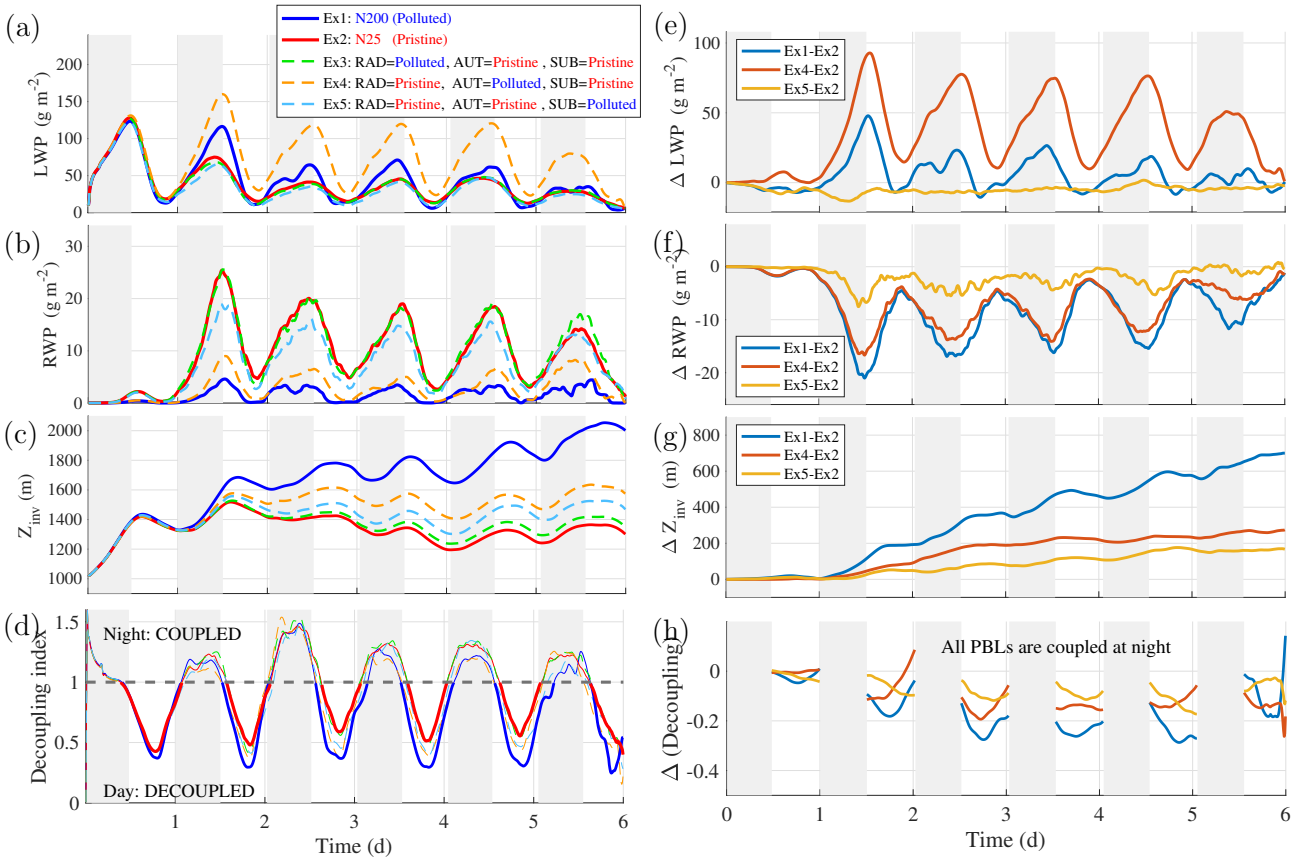

Figure 5. Results of sensitivity experiments for two most extreme droplet number concentrations, Polluted (200/cc) and Pristine (25/cc), applied independently to three main model components: radiation (RAD), rain autoconversion (AUT), and cloud water subsidence (SUB). The panels show time series of: (a) LWP and (e) its difference between three pairs of key experiments (Ex1-Ex2, Ex4-Ex2, Ex5-Ex2); (b) RWP and (f) its difference; (c) inversion height and (g) its difference; (d) PBL decoupling and (h) its difference, omitting night time when all PBLs are coupled. To reduce noise and extract the main signal, the LWP/RWP, and decoupling index time series are smoothed using a 5-hour (the former) and an 8-hour (the latter) window.